

A Fourier–Karhunen–Loève discretization scheme for stationary random material properties in SFEM

C. F. Li¹, Y. T. Feng^{1,*},[†], D. R. J. Owen¹, D. F. Li² and I. M. Davis³

¹*Civil & Computational Engineering Centre, School of Engineering, University of Wales Swansea, Swansea SA2 8PP, U.K.*

²*LASMIS, Universite de Technologie de Troyes, 12 rue Marie Curie, BP 2060, 10010 Troyes, France*

³*Department of Mathematics, University of Wales Swansea, Swansea SA2 8PP, U.K.*

SUMMARY

In order to overcome the computational difficulties in Karhunen–Loève (K–L) expansions of stationary random material properties in stochastic finite element method (SFEM) analysis, a Fourier–Karhunen–Loève (F–K–L) discretization scheme is developed in this paper, by following the harmonic essence of stationary random material properties and solving a series of specific technical challenges encountered in its development. Three numerical examples are employed to investigate the overall performance of the new discretization scheme and to demonstrate its use in practical SFEM simulations. The proposed F–K–L discretization scheme exhibits a number of advantages over the widely used K–L expansion scheme based on FE meshes, including better computational efficiency in terms of memory and CPU time, convenient *a priori* error-control mechanism, better approximation accuracy of random material properties, explicit methods for predicting the associated eigenvalue decay speed and geometrical compatibility for random medium bodies of different shapes. Copyright © 2007 John Wiley & Sons, Ltd.

Received 2 August 2005; Revised 11 June 2007; Accepted 5 July 2007

KEY WORDS: stochastic finite element method; random media

1. INTRODUCTION

1.1. Background of discretization of random material properties

Due to the increasing demand for quantitative analysis of practical engineering systems consisting of random media (e.g. rocks, concrete and composite materials with random inclusions) and also due to the continual exponential increase in computer power and data storage, the study

*Correspondence to: Y. T. Feng, Civil & Computational Engineering Centre, School of Engineering, University of Wales Swansea, Swansea SA2 8PP, U.K.

[†]E-mail: y.feng@swan.ac.uk

Contract/grant sponsor: EPSRC; contract/grant numbers: GR/R87222, GR/R92318

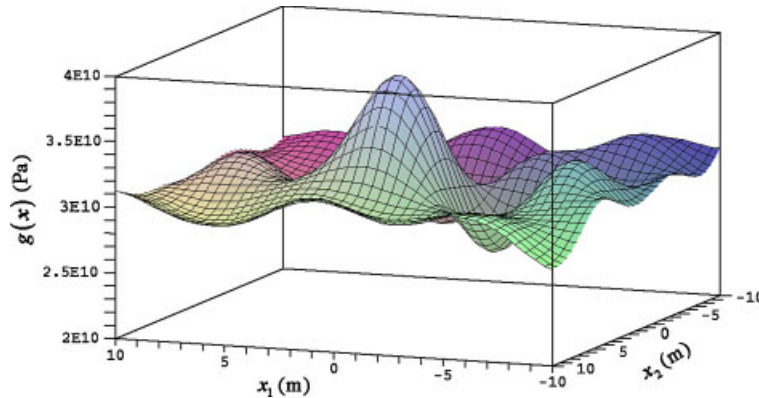


Figure 1. Young's modulus of a random medium plate.

of stochastic finite element methods (SFEMs) [1–20] has developed steadily over the past two decades. A major issue for setting up a SFEM simulation for practical random medium systems is to effectively discretize the irregular variation of material properties through the medium. Figure 1 plots a simple example of random material properties to be discretized, and $g(\mathbf{x})$ denotes a particular variation in Young's modulus of a random medium plate.

Over the last few decades, various methods have been developed for the discretization of random material properties, and they include the middle point method [1, 2], the local averaging method [3], the shape function method [4–6], the least-squares discretization method [7] and the trigonometric series approximation method [8–11]. However, some of these are either inefficient (measured by the total number of random variables required) or inaccurate (measured by the error between the interpolated stochastic field and the real one) for an advanced SFEM formulation. Some critical reviews on this subject can be found in [7, 9, 13, 20].

To date, the most significant step forward for the above stochastic-field discretization problem is the application of Karhunen–Loève (K–L) expansions [21], which was first introduced into SFEM research by Spanos and Ghanem [12], and since then has been widely used in various SFEM formulations [13–20] to discretize random material properties. However, as outlined in the next subsection, several computational issues arise in further applications of K–L expansions to practical random medium problems.

1.2. Motivation of this paper

In this paper, symbols \mathbb{R} , \mathbb{Z} and \mathbb{N} are exclusively used with their standard meanings, i.e. \mathbb{R} denotes the real number set, \mathbb{Z} the integer set and $\mathbb{N} \triangleq \{1, 2, 3, \dots\}$ the natural number set. Symbols ω , δ_{ij} and $\overline{(\cdot)}$ represent, respectively, a basic random event, the Kronecker delta and the complex conjugate. Superscript T denotes the transpose of a matrix or a vector. Integer $n = 1, 2, 3$ denotes the dimensionality of the problem's spatial domain, and a term n -interval is used to, respectively, denote an interval in 1D cases, a rectangle in 2D cases or a cuboid in 3D cases.

Let $D \subset \mathbb{R}^n$ be a random medium body with the random material property denoted by $H(\mathbf{x}, \omega)$ $\mathbf{x} \in D$, a second-order stochastic field [21] initially defined by its expectation function $H_0(\mathbf{x}) \triangleq E(H(\mathbf{x}, \omega))$ and a covariance function $R(\mathbf{x}_1, \mathbf{x}_2) \triangleq \text{Cov}(H(\mathbf{x}_1, \omega), H(\mathbf{x}_2, \omega))$. Following

the K–L expansion theorem [21], $H(\mathbf{x}, \omega)$ can be discretized as

$$H(\mathbf{x}, \omega) = H_0(\mathbf{x}) + \sum_{i=1}^{+\infty} \sqrt{\lambda_i} \zeta_i(\omega) \psi_i(\mathbf{x}) \quad (1)$$

where the random variables $\zeta_i(\omega)$ satisfy $E(\zeta_i(\omega)) = 0$ and $E(\zeta_i(\omega) \overline{\zeta_j(\omega)}) = \delta_{ij}$, and the deterministic constants λ_i and functions $\psi_i(\mathbf{x})$ are eigenvalues and eigenfunctions of the characteristic equation

$$\int_D R(\mathbf{x}_1, \mathbf{x}_2) \psi(\mathbf{x}_1) d\mathbf{x}_1 = \lambda \psi(\mathbf{x}_2) \quad (2)$$

such that $\lambda_i > 0$ and $\int_D \psi_i(\mathbf{x}) \overline{\psi_j(\mathbf{x})} d\mathbf{x} = \delta_{ij}$. In a numerical treatment, Equation (1) is truncated into a finite series after sorting λ_i in a descending order, and by using the trace relation

$$\sum_{i=1}^{+\infty} \lambda_i = \int_D R(\mathbf{x}, \mathbf{x}) d\mathbf{x} \quad (3)$$

the length of the series can be determined by the required accuracy of the total variance. In the sense of mean-square convergence, the finite K–L series truncated from (1) then provides an optimal linear representation for keeping the subspace that has the minimum variance of error.

It is clear that successful applications of K–L expansions in practical problems crucially rely on the existence of efficient and accurate methods to solve for the required eigenstructures of stochastic fields. In the SFEM literature, the integral equation (2) is usually solved by the standard Galerkin finite element method (FEM) (see e.g. [13, 18]), and the same FE mesh is adopted for the solution of the governing partial differential equations (PDEs) of the physical system. This leads to a generalized algebraic eigenvalue problem

$$\mathbf{A}\mathbf{v} = \lambda\mathbf{B}\mathbf{v} \quad (4)$$

in which \mathbf{A} is a full matrix (real symmetric and non-negative definite), \mathbf{B} a sparse matrix (real symmetric and positive definite), and λ and \mathbf{v} denote, respectively, the unknown eigenvalue and eigenvector. Unfortunately, several computational difficulties are encountered when solving the K–L eigenpairs in various SFEM simulations [12–18]:

- The associated computational costs mainly include two parts: constructing the full matrix \mathbf{A} and solving for the corresponding generalized eigenproblem. These operations can be very challenging [18], in terms of both memory and CPU time, because the dimension of the full matrix \mathbf{A} equals the total number of FE nodes and a large number of elements are required to achieve a reasonable K–L solution for practical random media, of which the ratio between material size and the effective correlation length is often greater than 10.
- The computational error of the K–L eigenpairs and hence of the K–L representation for random material properties relies largely on the density of the FE mesh involved. It is generally difficult to predict and control the resulting approximation error unless appropriate adaptive re-meshing algorithms are employed.
- The approximation error of the eigenfunctions $\psi_i(\mathbf{x})$ is relatively poor [13] due to the lack of an effective *a priori* error-control mechanism in the K–L representation based on FE meshes, although the error of eigenvalues λ_i can be partially managed using Equation (3).

- In engineering analysis of practical random medium systems, it is desirable to make a pre-estimate of the overall computational cost of the SFEM simulation, which is very much determined by the total number of random variables included in the corresponding mathematical model. However, an effective method to predict the minimum number of random variables required in the K–L representation to satisfy the given discretization accuracy of random material properties has not been available in the current literature.

These computational difficulties have hampered further applications of K–L expansions in practical random medium problems, in particular for large random media and small effective correlation length. It is this concern that motivates the current work, and a Fourier–Karhunen–Loève (F–K–L) discretization scheme for stationary random material properties is presented in this paper. The discretization problem is first analysed in the light of the existing mathematical results in Section 2. Section 3 introduces the F–K–L discretization scheme with the solutions of a sequence of specific technical problems encountered in its development, following which some useful properties are derived in Section 4.

2. PROBLEM ANALYSIS

In the K–L expansion (1), the probability distribution of $\xi_i(\omega)$ remains undetermined unless $H(\mathbf{x}, \omega)$ is a Gaussian field, for which $\xi_i(\omega)$ are Gaussian random variables [21]. The first two statistical moments of $H(\mathbf{x}, \omega)$ are insufficient to fully define a general second-order stochastic field, and additional information must be provided in order to determine the probability distribution of $\xi_i(\omega)$. This important issue is, however, out of the scope of this paper. Nevertheless, due to the central limit theorem, the Gaussian assumption may be approximately satisfied in many engineering problems and therefore widely adopted [11, 13]. In this work, whenever the probability distribution of $\xi_i(\omega)$ is needed, $H(\mathbf{x}, \omega)$ is assumed to be a Gaussian field.

For the description of random material properties, the wide-sense stationary (or briefly stationary) stochastic field [21–23] is one of the most widely used types of stochastic fields in the SFEM literature [1–20]. It should be noted that the K–L expansion holds for any second-order stochastic field, but this paper considers only stationary random material properties. In this special case, the expectation and covariance functions of $H(\mathbf{x}, \omega)$ degenerate, respectively, into $H_0(\mathbf{x}) = H_0$ and $R(\mathbf{x}_1, \mathbf{x}_2) = R(\mathbf{x}_1 - \mathbf{x}_2) = R(\boldsymbol{\tau})$. In mathematics, the eigenpair, λ_i and $\psi_i(\mathbf{x})$ in (1), is essentially the spectrum of the linear integral operator $(Tf)(\mathbf{x}_2) \triangleq \int_D R(\mathbf{x}_1, \mathbf{x}_2) f(\mathbf{x}_1) d\mathbf{x}_1$, which is very difficult to be obtained accurately if $H(\mathbf{x}, \omega)$ is a general second-order stochastic field. However, due to the harmonic essence of the stationary stochastic fields outlined below, it is possible to develop an accurate and efficient discretization scheme for stationary random material properties.

For the stationary stochastic field $H(\mathbf{x}, \omega)$, $\mathbf{x} \in \mathbb{R}^n$, whose covariance function is $R(\boldsymbol{\tau})$, the following spectral decompositions (see e.g. [22, 23]) hold:

$$H(\mathbf{x}, \omega) = H_0 + \int_{\mathbb{R}^n} e^{\sqrt{-1}\mathbf{x}\cdot\mathbf{y}} dZ(\mathbf{y}, \omega) \quad (5)$$

$$R(\boldsymbol{\tau}) = \int_{\mathbb{R}^n} e^{\sqrt{-1}\boldsymbol{\tau}\cdot\mathbf{y}} dF(\mathbf{y}) = \int_{\mathbb{R}^n} f(\mathbf{y}) e^{\sqrt{-1}\boldsymbol{\tau}\cdot\mathbf{y}} d\mathbf{y} \quad (6)$$

where $F(\mathbf{y})$ is a bounded, real-valued function satisfying $\int_A dF(\mathbf{y}) \geq 0$ for all measurable $A \subset \mathbb{R}^n$; $f(\mathbf{y}) > 0$ vanishes at infinity (i.e. $\lim_{\|\mathbf{y}\|_2 \rightarrow +\infty} f(\mathbf{y}) = 0$); and $Z(\mathbf{y}, \omega)$ satisfying

$$\begin{aligned} Z(-\infty, \omega) &= 0, & E(Z(\mathbf{y}, \omega)) &= 0 \\ E(|Z(\mathbf{y}, \omega)|^2) &= F(\mathbf{y}), & E(|dZ(\mathbf{y}, \omega)|^2) &= dF(\mathbf{y}) = f(\mathbf{y}) \, d\mathbf{y} \end{aligned} \tag{7}$$

is a complex-valued stochastic field with orthogonal increments (i.e. $E(Z(\mathbf{F}_1^n, \omega) \overline{Z(\mathbf{F}_2^n, \omega)}) = 0$ for any pair of disjoint n -intervals $\mathbf{F}_1^n, \mathbf{F}_2^n \subset \mathbb{R}^n$). In (5)–(6), both $H(\mathbf{x}, \omega)$ and $R(\tau)$ are expressed in the frequency space and in the form of the inverse Fourier transform. In particular, $F(\mathbf{y})$ is termed the spectral distribution function of $H(\mathbf{x}, \omega)$ and $R(\tau)$, and $f(\mathbf{y})$ is the associated spectral density function that can be readily obtained using the Fourier transform

$$f(\mathbf{y}) = \frac{1}{(2\pi)^n} \int_{\mathbb{R}^n} R(\tau) e^{-\sqrt{-1}\tau \cdot \mathbf{y}} \, d\tau \tag{8}$$

Clearly, by approximating the infinite integrations in (5)–(6) with finite summations, a stationary stochastic field defined in \mathbb{R}^n can be expressed as a finite series of general trigonometric functions. For instance, a real-valued stationary stochastic field $h(x, \omega)$, $x \in \mathbb{R}$ with mean zero and spectral density function $f_h(y)$ can be approximated by $\sum_{i=1}^q \sigma_i (A_i(\omega) \cos(y_i x) + B_i(\omega) \sin(y_i x))$, where $\sigma_i^2 = \int_{y_k - \Delta y/2}^{y_k + \Delta y/2} f_h(y) \, dy$, $A_i(\omega)$ and $B_i(\omega)$ are uncorrelated random variables with mean zero and variance one. Since no equation solving is involved, this trigonometric series approximation scheme and its improvements have long been applied in the SFEM (mainly in Monte Carlo simulations [8–11] to generate material samples) in an intuitive manner. However, in order to ensure the convergence of such a general trigonometric series, the integration domain in (5)–(6) has to be truncated at a sufficiently large domain in the frequency space while the summation steps have to be set sufficiently small, which in turn makes this simple scheme inefficient for practical uses. Moreover, the continual spectrum in (5)–(8) is not particularly useful for model reduction in SFEM analysis.

In fact, applying Equation (8) to calculate the following integration yields

$$\begin{aligned} \int_{\mathbb{R}^n} R(\mathbf{x}_1 - \mathbf{x}_2) e^{-\sqrt{-1}\mathbf{x}_1 \cdot \mathbf{y}} \, d\mathbf{x}_1 &= e^{-\sqrt{-1}\mathbf{x}_2 \cdot \mathbf{y}} \int_{\mathbb{R}^n} R(\mathbf{x}_1 - \mathbf{x}_2) e^{-\sqrt{-1}(\mathbf{x}_1 - \mathbf{x}_2) \cdot \mathbf{y}} \, d\mathbf{x}_1 \\ &= (2\pi)^n f(\mathbf{y}) e^{-\sqrt{-1}\mathbf{x}_2 \cdot \mathbf{y}} \end{aligned} \tag{9}$$

The above characteristic equation is satisfied for all $\mathbf{y} \in \mathbb{R}^n$. More importantly, by comparing (9) with (2), it is clear that, without solving Equation (2), expressions (5)–(6) provide an explicit solution for the K–L expansion of $H(\mathbf{x}, \omega)$, $\mathbf{x} \in \mathbb{R}^n$ in terms of Fourier integrals. Specifically, $dZ(\mathbf{y}, \omega)$ and $e^{\sqrt{-1}\mathbf{x} \cdot \mathbf{y}}$ in (5) correspond, respectively, to $\sqrt{\lambda_i} \zeta_i(\omega)$ and $\psi_i(\mathbf{x})$ in (1), and the continual spectrum indexed by \mathbf{y} corresponds to the discrete spectrum indexed by i . The connection between the K–L expansion (1)–(3) and the spectral representation theory (5)–(8) has long been recognized in applied mathematics and signal processing (see, e.g. [24]), and the recognition is vital to the investigation of asymptotic properties of the solution for Equation (2) in stationary cases and is also useful for the derivation of exact solutions for Equation (2) in several special cases.

In SFEM analysis, specifically for the K–L discretization of random material properties, it is required to numerically obtain the discrete spectrum of Equation (2) in finite domain. However, it

appears that the essential link indicated in (9) has not been fully appreciated in the SFEM community, but instead the FEM has almost always been adopted in the solution of the corresponding characteristic equation, in many of which the random material property involved is essentially stationary [12–20]. The advantage of the F–K–L approach is obvious in that the same mesh with the following mechanical analysis can be employed, which in turn minimizes the extra work in mesh generation and stiffness-matrix computation. However, as highlighted in Section 1.2, several unsatisfactory computational issues arise. Hence, inspired by the harmonic essence of stationary stochastic fields (5)–(9), a meshfree F–K–L discretization scheme is introduced in the next section and a sequence of specific technical problems encountered in its development are solved. It will be shown that, for stationary random material properties, the F–K–L discretization scheme resolves all the computational problems previously addressed.

3. THE F–K–L DISCRETIZATION SCHEME

3.1. Fourier expansion of stationary random material properties

As the random material property $H(\mathbf{x}, \omega)$, $\mathbf{x} \in D$ of the random medium body $D \subset \mathbb{R}^n$ is assumed stationary, the discretization problem can alternatively be considered in an n -interval $\mathbf{T}^n \triangleq \{\mathbf{x} = (x_1, \dots, x_n) \in \mathbb{R}^n \mid -t_k \leq x_k \leq t_k, t_k > 0 \ (k = 1, \dots, n)\} \supset D$ with volume $V_{\mathbf{T}^n} = 2^n \prod_{k=1}^n t_k$. Note that the Fourier integral and series [25] are essentially equivalent, except that the former is defined in \mathbb{R}^n but the latter is defined in an n -interval. The inverse Fourier transform (5) of $H(\mathbf{x}, \omega)$, $\mathbf{x} \in \mathbb{R}^n$ infers the following complex Fourier expansion of $H(\mathbf{x}, \omega)$, $\mathbf{x} \in \mathbf{T}^n$:

$$H(\mathbf{x}, \omega) = H_0 + \sum_{m_1=-\infty}^{+\infty} \dots \sum_{m_n=-\infty}^{+\infty} \Delta Z(\mathbf{m}, \omega) e^{\sqrt{-1} \sum_{k=1}^n m_k \theta_k x_k} \tag{10}$$

where $\mathbf{m} = (m_1, \dots, m_n) \in \mathbb{Z}^n$; $\theta_k = \pi/t_k, k = 1, \dots, n$; $e^{\sqrt{-1} \sum_{k=1}^n m_k \theta_k x_k}$ constitute the Fourier basis defined in \mathbf{T}^n ; and $\Delta Z(\mathbf{m}, \omega) = 1/V_{\mathbf{T}^n} \int_{\mathbf{T}^n} (H(\mathbf{x}, \omega) - H_0) e^{-\sqrt{-1} \sum_{k=1}^n m_k \theta_k x_k} d\mathbf{x}$ are complex-valued random Fourier coefficients. The convergence and well posedness of (10) are ensured by the completeness and orthogonality of the Fourier basis. It is then obvious that $E(\Delta Z(\mathbf{m}, \omega)) = 0$.

Although the stochastic field $Z(\mathbf{y}, \omega)$ in (5) is with orthogonal increments, the random variable sequence $\Delta Z(\mathbf{m}, \omega)$ in (10) is not necessarily (and usually is not) composed of orthogonal random variables. This is because of the simplification from the Fourier integrals to the Fourier series; the frequency of the trigonometric functions in (10) is preset by \mathbf{m} and, consequently, random coefficients $\Delta Z(\mathbf{m}, \omega)$ must be adapted for the convergence of the infinite Fourier series, for which the strictly orthogonal property of $Z(\mathbf{y}, \omega)$ is inevitably destroyed. Hence, Equation (10) is *not* the K–L expansion of $H(\mathbf{x}, \omega)$, $\mathbf{x} \in \mathbf{T}^n$.

In a numerical formulation, the convergent Fourier series (10) is truncated such that

$$\begin{aligned} H(\mathbf{x}, \omega) &\approx H_0 + \sum_{m_1=-M_1}^{M_1} \dots \sum_{m_n=-M_n}^{M_n} \Delta Z(\mathbf{m}, \omega) e^{\sqrt{-1} \sum_{k=1}^n m_k \theta_k x_k} \\ &= H_0 + \Delta \mathbf{Z}^T(\omega) \mathbf{e}(\mathbf{x}) = H_N(\mathbf{x}, \omega) \end{aligned} \tag{11}$$

where $\mathbf{M} = (M_1, \dots, M_n) \in \mathbb{N}^n$; $N = \prod_{k=1}^n (2M_k + 1)$; and vectors $\Delta \mathbf{Z}(\omega)$ and $\mathbf{e}(\mathbf{x})$ are, respectively, constructed from $\sqrt{V_{\mathbf{T}^n}} \Delta Z(\mathbf{m}, \omega)$ and $e^{\sqrt{-1} \sum_{k=1}^n m_k \theta_k x_k} / \sqrt{V_{\mathbf{T}^n}}$. The constant coefficient

$\sqrt{V_{\mathbf{T}^n}}$ is chosen to normalize the Fourier basis, and the entries in $\Delta\mathbf{Z}(\omega)$ and $\mathbf{e}(\mathbf{x})$ are organized in an ascending order of the frequency number \mathbf{m} .

The truncation error $\varepsilon_N \triangleq |H(\mathbf{x}, \omega) - H_N(\mathbf{x}, \omega)|$ of the Fourier approximation (11) depends on the integer domain $\mathbf{M}^n \triangleq \{\mathbf{m} \in \mathbb{Z}^n \mid -M_k \leq m_k \leq M_k (k = 1, \dots, n)\}$, whose boundary is \mathbf{M} . Thus, in order to have an explicit control of ε_N , \mathbf{M} must be determined according to the required accuracy of $H(\mathbf{x}, \omega)$. This can be achieved using the spectral representation of $R(\boldsymbol{\tau})$, and the details are given below.

The covariance function of $H_N(\mathbf{x}, \omega)$ is

$$R_N(\boldsymbol{\tau}) = E \left(\left(\sum_{m_1=-M_1}^{M_1} \dots \sum_{m_n=-M_n}^{M_n} \Delta Z(\mathbf{m}, \omega) e^{\sqrt{-1} \sum_{k=1}^n m_k \theta_k x_{1k}} \right) \times \overline{\left(\sum_{m_1=-m_1}^{M_1} \dots \sum_{m_n=-M_n}^{M_n} \Delta Z(\mathbf{m}, \omega) e^{\sqrt{-1} \sum_{k=1}^n m_k \theta_k x_{2k}} \right)} \right) \tag{12}$$

and its right-hand side term with the highest frequency is

$$E(\Delta Z(\mathbf{M}, \omega) e^{\sqrt{-1} \sum_{k=1}^n M_k \theta_k x_{1k}} \overline{\Delta Z(\mathbf{M}, \omega) e^{\sqrt{-1} \sum_{k=1}^n M_k \theta_k x_{2k}}}) = E(\Delta Z(\mathbf{M}, \omega) \overline{\Delta Z(\mathbf{M}, \omega)}) e^{\sqrt{-1} \sum_{k=1}^n M_k \theta_k (x_{1k} - x_{2k})} \tag{13}$$

Hence, as indicated by $(m_1\theta_1, \dots, m_n\theta_n)$, $R_N(\boldsymbol{\tau})$ has a discrete frequency domain whose boundary is $(M_1\theta_1, \dots, M_n\theta_n)$. Let $\mathbf{F}^n \triangleq \{\mathbf{y} \in \mathbb{R}^n \mid -f_k \leq y_k \leq f_k, f_k > 0 (k = 1, \dots, n)\}$ denote the smallest domain in the frequency space of $R(\boldsymbol{\tau})$ such that

$$\frac{\int_{\mathbf{F}^n} f(\mathbf{y}) \, d\mathbf{y}}{\int_{\mathbb{R}^n} f(\mathbf{y}) \, d\mathbf{y}} = \frac{\int_{\mathbf{F}^n} f(\mathbf{y}) \, d\mathbf{y}}{R(\mathbf{0})} \geq \mu, \quad 0 < \mu < 1 \tag{14}$$

where constant μ is the required accuracy for approximating the spectrum identified by $f(\mathbf{y})$. In order to ensure that $H_N(\mathbf{x}, \omega)$ satisfies the given accuracy μ , the discrete frequency domain of $R_N(\boldsymbol{\tau})$ needs to be set in accordance with the continual frequency domain of $R(\boldsymbol{\tau})$. Therefore, the relation

$$(M_k - 1)\theta_k < f_k \leq M_k\theta_k, \quad k = 1, \dots, n \tag{15}$$

holds between frequency boundaries $(M_1\theta_1, \dots, M_n\theta_n)$ and \mathbf{F}^n , which further leads to

$$M_k = \left\lceil \frac{f_k}{\theta_k} \right\rceil = \left\lceil \frac{f_k t_k}{\pi} \right\rceil, \quad k = 1, \dots, n \tag{16}$$

where operator $\lceil x \rceil$ gives the minimum integer that is not less than x .

Regarding the above Fourier expansion of stationary random material properties, the following two remarks can be made in order. Firstly, it is well known that the Fourier transforms of many typical functions can be obtained analytically; therefore, the spectral density function $f(\mathbf{y})$ (8) can be obtained exactly for many typical $R(\boldsymbol{\tau})$ encountered in practice. If this is not the case, the standard fast Fourier transform (FFT) can be applied to numerically calculate $f(\mathbf{y})$. Secondly, according to the well-known Heisenberg inequality [25] in Fourier analysis, a wider $R(\boldsymbol{\tau})$, which corresponds approximately to a larger effective correlation length, results in a narrower $f(\mathbf{y})$, which

approximately corresponds to a smaller major frequency domain \mathbf{F}^n ; and *vice versa*. Consequently, from (16), \mathbf{M}^n expands with the growth of the random medium domain, but normally shrinks as the effective correlation length increases; and *vice-versa*.

3.2. Principal component analysis of the Fourier expansion

In (11), in terms of the fixed Fourier vector $\mathbf{e}(\mathbf{x})$, $H_N(\mathbf{x}, \omega) - H_0$ is represented by the random vector $\Delta\mathbf{Z}(\omega)$, whose entries $\Delta Z(\mathbf{m}, \omega)$ are not strictly orthogonal to each other. Hence, due to the orthogonality of Fourier basis, the standard dimensionality reduction technique of principal component analysis (PCA) can be performed to orthogonalize $\Delta\mathbf{Z}(\mathbf{m}, \omega)$ and further improve the efficiency of the Fourier expansion. The PCA operation for $\Delta\mathbf{Z}(\omega)$ is formulated below, and the general theoretical background of PCA can be found in standard textbooks, e.g. [26].

Let $\mathbf{G} = E(\Delta\mathbf{Z}(\omega)\Delta\mathbf{Z}^T(\omega))$ denote the covariance matrix of $\Delta\mathbf{Z}(\omega)$, $e_i(\mathbf{x})$ the i th term of $\mathbf{e}(\mathbf{x})$ and $\Delta Z_i(\omega)$ the i th term of $\Delta\mathbf{Z}(\omega)$. Then, the matrix \mathbf{G} can be constructed from

$$\begin{aligned} \mathbf{G}_{ij} &= \text{Cov}(\Delta Z_i(\omega), \Delta Z_j(\omega)) \\ &= \int_{\mathbf{T}^n} \int_{\mathbf{T}^n} R(\mathbf{x}_1 - \mathbf{x}_2) \overline{e_i(\mathbf{x}_1)} e_j(\mathbf{x}_2) \, d\mathbf{x}_1 \, d\mathbf{x}_2 \\ &= \frac{1}{V_{\mathbf{T}^n}} \int_{\mathbf{T}^n} \int_{\mathbf{T}^n} R(\mathbf{x}_1 - \mathbf{x}_2) e^{-\sqrt{-1} \sum_{k=1}^n m_{ik} \theta_k x_{1k}} e^{\sqrt{-1} \sum_{k=1}^n m_{jk} \theta_k x_{2k}} \, d\mathbf{x}_1 \, d\mathbf{x}_2 \end{aligned} \tag{17}$$

where \mathbf{G}_{ij} is the entry at the i th row and j th column of \mathbf{G} . Due to the symmetric and non-negative definite properties of $R(\mathbf{x}_1 - \mathbf{x}_2)$ [21–23], \mathbf{G} is a non-negative-definite Hermitian matrix.

It is observed from Equation (17) that each entry of matrix \mathbf{G} is an integral of multidimensional oscillatory functions, for which standard numerical integration algorithms [27] such as Clenshaw–Curtis quadrature method, Gaussian quadrature method and Filon’s integration have very poor performance and may even cease to be useful in 2D and 3D random medium problems. Consequently, although the form of (17) is clear, it is not particularly useful for the calculation of \mathbf{G} , and further transformation is necessary. Substituting (6) into (17) yields

$$\mathbf{G}_{ij} = \frac{2^n}{V_{\mathbf{T}^n}} \int_{\mathbb{R}^n} f(\mathbf{y}) \prod_{k=1}^n \frac{\cos((m_{jk} - m_{ik})\pi) - \cos(2y_k t_k - (m_{ik} + m_{jk})\pi)}{\left(y_k - m_{ik} \frac{\pi}{t_k}\right) \left(y_k - m_{jk} \frac{\pi}{t_k}\right)} \, d\mathbf{y} \tag{18}$$

and, furthermore, substituting (8) into the above equation yields

$$\begin{aligned} \mathbf{G}_{ij} &= \frac{1}{\pi^n V_{\mathbf{T}^n}} \int_{\mathbb{R}^n} R(\boldsymbol{\tau}) \\ &\quad \times \left(\prod_{k=1}^n \int_{\mathbb{R}} \frac{\cos((m_{jk} - m_{ik})\pi) - \cos(2y_k t_k - (m_{ik} + m_{jk})\pi)}{\left(y_k - m_{ik} \frac{\pi}{t_k}\right) \left(y_k - m_{jk} \frac{\pi}{t_k}\right)} e^{-\sqrt{-1} y_k \tau_k} \, dy_k \right) \, d\boldsymbol{\tau} \end{aligned} \tag{19}$$

After explicitly calculating the inner integral in the above equation, which is a standard 1D Fourier transform, the resulting expression can be simplified as

$$\mathbf{G}_{ij} = \int_0^{2t_1} \cdots \int_0^{2t_n} \tilde{R}(\boldsymbol{\tau}) \left(\prod_{k=1}^n A_{ijk}(\tau_k) B_{ijk}(\tau_k) \right) d\boldsymbol{\tau} \tag{20}$$

in which

$$A_{ijk}(\tau_k) = \begin{cases} 2 - \frac{\tau_k}{t_k}, & m_{ik} = m_{jk} \\ \frac{(-1)^{m_{ik}+m_{jk}}}{(m_{ik} - m_{jk})\pi}, & m_{ik} \neq m_{jk} \end{cases} \tag{21}$$

$$B_{ijk}(\tau_k) = \begin{cases} \cos\left(m_{ik} \frac{\pi}{t_k} \tau_k\right), & m_{ik} = m_{jk} \\ \sin\left(m_{jk} \frac{\pi}{t_k} \tau_k\right) - \sin\left(m_{ik} \frac{\pi}{t_k} \tau_k\right), & m_{ik} \neq m_{jk} \end{cases} \tag{22}$$

and

$$\tilde{R}(\boldsymbol{\tau}) = \frac{1}{2^n} \sum_{k_1=1}^2 \cdots \sum_{k_n=1}^2 R((-1)^{k_1} \tau_1, \dots, (-1)^{k_n} \tau_n) \tag{23}$$

is the axis-symmetric component of $R(\boldsymbol{\tau})$.

Note that in (20)–(23), all the entries in \mathbf{G} are essentially Fourier coefficients of $\tilde{R}(\boldsymbol{\tau}) \prod_{k=1}^n A_{ijk}(\tau_k)$, and up to a constant scalar determined by i and j there are only 2^n possible forms of $\tilde{R}(\boldsymbol{\tau}) \prod_{k=1}^n A_{ijk}(\tau_k)$. Hence, the covariance matrix can be efficiently constructed by using the FFT [28], and the computational cost is $O(2^n N \log N)$. It is worth noting that the right-hand side of (20) may be analytically obtained for some typical covariance functions encountered in practice.

From (20)–(23), it is observed that the matrix \mathbf{G} is real and symmetric. Hence, the non-negative-definite Hermitian matrix \mathbf{G} is specifically real-symmetric and non-negative definite. Therefore, there exists an orthogonal matrix $\mathbf{Q}^{-1} = \mathbf{Q}^T$ such that

$$\mathbf{Q}^T \mathbf{G} \mathbf{Q} = \text{diag}(\lambda_1, \lambda_2, \dots, \lambda_N) \tag{24}$$

where $\lambda_1 \geq \lambda_2 \geq \dots \geq \lambda_N \geq 0$. The calculation of \mathbf{Q} and λ_i is a standard algebraic eigenvalue problem. Furthermore, the matrix \mathbf{G} can be transformed into a block-diagonal matrix containing two blocks, and the dimensionality of each block matrix is approximately half of the dimensionality of \mathbf{G} . The proof for the block-diagonal property of \mathbf{G} is outlined below.

In (17)–(20), \mathbf{G} is constructed with respect to the complex Fourier basis $e^{\sqrt{-1} \sum_{k=1}^n m_k \theta_k x_k} / \sqrt{V_{\mathbf{T}^n}}$, and, equivalently, the covariance matrix can be constructed with respect to the real Fourier basis

$$1/\sqrt{V_{\mathbf{T}^n}}/2 \left\{ \frac{1}{\sqrt{2}}, \cos \sum_{k=1}^n m_k \theta_k x_k, \sin \sum_{k=1}^n m_k \theta_k x_k \right\}$$

Noting that

$$\cos \left(\sum_{k=1}^n m_k \theta_k x_k \right) = \frac{e^{\sqrt{-1} \sum_{k=1}^n m_k \theta_k x_k} + e^{-\sqrt{-1} \sum_{k=1}^n m_k \theta_k x_k}}{2} \tag{25a}$$

and

$$\sin \left(\sum_{k=1}^n m_k \theta_k x_k \right) = \frac{e^{\sqrt{-1} \sum_{k=1}^n m_k \theta_k x_k} - e^{-\sqrt{-1} \sum_{k=1}^n m_k \theta_k x_k}}{2\sqrt{-1}} \tag{25b}$$

the covariance matrix based on the real Fourier basis can be obtained from \mathbf{G} via an orthogonal transformation. Furthermore, consider the following entry:

$$2/V_{\mathbf{T}^n} \int_{\mathbf{T}^n} \int_{\mathbf{T}^n} R(\mathbf{x}_1 - \mathbf{x}_2) \left(\cos \sum_{k=1}^n m_{i_k} \theta_k x_{1k} \right) \left(\sin \sum_{k=1}^n m_{j_k} \theta_k x_{2k} \right) d\mathbf{x}_1 d\mathbf{x}_2 \tag{26}$$

in the covariance matrix based on the real Fourier basis. The above expression is obviously real-valued, and also, according to (17), (20) and (25), its real part is zero. Hence, all the coupled entries of the form of (27) are zero. This decoupling between sine terms and cosine terms infers that the covariance matrix based on the real Fourier basis can be organized as a block-diagonal matrix with two blocks: one block is constructed from the sine terms and the other block is constructed from the cosine terms together with the constant term.

The algebraic eigenstructure of \mathbf{G} can be readily obtained by using existing eigensolvers. Once \mathbf{Q} and λ_i ($i = 1, \dots, N$) are obtained, the eigenfunctions $\psi_i(\mathbf{x})$ and eigenvalues $\xi_i(\omega)$ can be constructed as follows:

$$\boldsymbol{\Psi}(\mathbf{x}) = (\psi_1(\mathbf{x}), \dots, \psi_N(\mathbf{x}))^T = \mathbf{Q}^T \mathbf{e}(\mathbf{x}) \tag{27}$$

$$\boldsymbol{\xi}(\omega) = (\xi_1(\omega), \dots, \xi_N(\omega))^T = \text{diag} \left(\frac{1}{\sqrt{\lambda_1}}, \dots, \frac{1}{\sqrt{\lambda_N}} \right) \mathbf{Q}^T \Delta \mathbf{Z}(\omega) \tag{28}$$

Then, it follows from Equation (11) that

$$H_N(\mathbf{x}, \omega) = H_0 + \sum_{i=1}^N \sqrt{\lambda_i} \xi_i(\omega) \psi_i(\mathbf{x}) \approx H_0 + \sum_{i=1}^{N^*} \sqrt{\lambda_i} \xi_i(\omega) \psi_i(\mathbf{x}) = H_{N^*}(\mathbf{x}, \omega) \tag{29}$$

in which N^* is the smallest integer such that

$$\frac{\sum_{i=1}^{N^*} \lambda_i}{\sum_{i=1}^N \lambda_i} \geq \mu^*, \quad 0 < \mu^* \leq 1 \tag{30}$$

where μ^* is the required accuracy for approximating the total variance of $H_N(\mathbf{x}, \omega)$.

3.3. The F–K–L discretization algorithm

Remark

Equation (29), together with (20)–(24) and (27)–(28), is termed the F–K–L discretization of stationary random material properties. Due to the completeness and orthogonality of the Fourier

basis and the PCA procedure, $H_{N^*}(\mathbf{x}, \omega)$ provides a series solution for the K–L expansion of $H(\mathbf{x}, \omega)$, $\mathbf{x} \in \mathbf{T}^n$. The total truncation error $\varepsilon_{N^*} = |H(\mathbf{x}, \omega) - H_{N^*}(\mathbf{x}, \omega)|$ is explicitly controlled by (14), (16) and (30); specifically, $\boldsymbol{\mu}$ controls the error of the spectrum (i.e. eigenvalues and eigenfunctions) of $H(\mathbf{x}, \omega)$ and μ^* controls the error of the total variance of $H(\mathbf{x}, \omega)$.

For a stationary random material property denoted by $H(\mathbf{x}, \omega)$, $\mathbf{x} \in D$, given the mean value H_0 , the covariance function $R(\boldsymbol{\tau})$ and the error-control parameters $\boldsymbol{\mu}$ and μ^* , the corresponding F–K–L discretization can be obtained with the following algorithm:

1. Find the minimum n -interval $\mathbf{T}^n \subset \mathbb{R}^n$ such that $D \subset \mathbf{T}^n$.
2. Determine \mathbf{M} , the boundary of \mathbf{M}^n , according to $\boldsymbol{\mu}$ and Equations (8), (14), (16).
3. Form the covariance matrix \mathbf{G} according to Equations (20)–(23).
4. Solve the standard algebraic eigenvalue problem with respect to \mathbf{G} to obtain \mathbf{Q} and λ_i .
5. Construct the F–K–L representation according to μ^* and Equations (27)–(30).

It is worth mentioning that for an irregular domain D the above F–K–L discretization constructed via the n -interval \mathbf{T}^n is not equivalent to the exact K–L expansion in D . Hence, in terms of the number of random variables contained in the series expression, the F–K–L representation may be less economical than the exact K–L expansion depending on the specific domain D .

The computational costs of the F–K–L discretization algorithm include two parts: (a) constructing the $N \times N$ covariance matrix \mathbf{G} and (b) solving the associated standard algebraic eigenvalue problem to obtain \mathbf{Q} and λ_i . For the former part, following Equations (20)–(23) and using FFT, the construction of \mathbf{G} is trivial. For the latter part, by using the decoupling technique addressed at the end of the previous subsection to transform \mathbf{G} into a block-diagonal matrix, the problem size of the associated algebraic eigenvalue problem can be reduced to half, which in turn significantly improves the computational efficiency of solving for \mathbf{Q} and λ_i (especially for large-scale covariance matrices \mathbf{G}). Consequently, the computational cost of the F–K–L discretization scheme can be expected to be very competitive.

4. PROPERTIES OF THE F–K–L DISCRETIZATION SCHEME

4.1. The diagonal F–K–L approximation scheme

It is observed in (20)–(23) that:

- (1) The integral kernel $A_{ijk}(\tau_k)$ is much larger in a diagonal entry of \mathbf{G} than in an off-diagonal entry; with the decreasing rate $1/\prod_{k=1}^n |m_{ik} - m_{jk}|$, it becomes increasingly smaller when the associated entry moves away from the matrix diagonal.
- (2) In practice, the function $\tilde{R}(\boldsymbol{\tau})$ usually exhibits its largest value at $\boldsymbol{\tau} = \mathbf{0}$ and decreases as $\|\boldsymbol{\tau}\|_2$ increases. Therefore, the major non-zero domain of $\tilde{R}(\boldsymbol{\tau})$ is the vicinity of the origin, in which $B_{ijk}(\tau_k)$ is much larger in a diagonal entry than in an off-diagonal entry depending on the decay rate of $\tilde{R}(\boldsymbol{\tau})$.

Following these two observations, it is concluded from (20) that the diagonal entries of the covariance matrix \mathbf{G} are usually much larger than the corresponding off-diagonal entries, i.e.

$$|\mathbf{G}_{ii}| \gg |\mathbf{G}_{ij}|, \quad i \neq j \quad (31)$$

The above property infers that $\Delta Z_i(\omega)$ are, in most cases, nearly orthogonal to each other, which further implies that $\Delta Z_i(\omega)$ and $e_i(\mathbf{x})$ provide a good initial estimate to the eigenstructure of $H(\mathbf{x}, \omega)$, $\mathbf{x} \in \mathbf{T}^n$. This insight makes it interesting to investigate the following stochastic field constructed only from the diagonal entries of \mathbf{G} :

$$H_d(\mathbf{x}, \omega) = H_0 + \sum_{i=1}^{+\infty} \Delta \tilde{Z}_i(\omega) e_i(\mathbf{x}) \tag{32}$$

where $E(\Delta \tilde{Z}_i(\omega)) = 0$ and $E(\Delta \tilde{Z}_i(\omega) \overline{\Delta \tilde{Z}_j(\omega)}) = \delta_{ij} E(\Delta Z_i(\omega) \overline{\Delta Z_j(\omega)})$.

Using (21)–(22), the covariance function of $H_d(\mathbf{x}, \omega)$ can be obtained as

$$\begin{aligned} & \text{Cov}(H_d(\mathbf{x}_1, \omega), H_d(\mathbf{x}_2, \omega)) \\ &= \frac{1}{V_{\mathbf{T}^n}} \sum_{m_1=-\infty}^{+\infty} \cdots \sum_{m_n=-\infty}^{+\infty} \left(\int_0^{2t_1} \cdots \int_0^{2t_n} \tilde{R}(\boldsymbol{\tau}) \left(\prod_{k=1}^n \left(2 - \frac{\tau_k}{t_k} \right) \cos \left(m_k \frac{\pi}{t_k} \tau_k \right) \right) d\boldsymbol{\tau} \right) \\ & \quad \times e^{\sqrt{-1} \sum_{k=1}^n m_k \theta_k (x_{1k} - x_{2k})} \\ &= R_d(\boldsymbol{\tau}) \end{aligned} \tag{33}$$

According to (32)–(33), $H_d(\mathbf{x}, \omega)$ is a stationary stochastic field with the same expectation function as $H(\mathbf{x}, \omega)$. Naturally, it is expected that $R_d(\boldsymbol{\tau})$ approximates $R(\boldsymbol{\tau})$ in a certain sense such that the diagonal F–K–L approximation $H_d(\mathbf{x}, \omega)$ can provide a reasonable estimate of $H(\mathbf{x}, \omega)$.

According to the Fourier expansion in (33), $R_d(\boldsymbol{\tau})$ is essentially the axis-symmetric component of $\tilde{R}(\boldsymbol{\tau}) \prod_{k=1}^n (2 - \tau_k/t_k)$. In addition, $R_d(\boldsymbol{\tau})$ has a period of \mathbf{T}^n ; therefore, it is necessary to consider only the behaviour of $R_d(\boldsymbol{\tau})$ in one half of \mathbf{T}^n ; that is,

$$\begin{aligned} R_d(\boldsymbol{\tau}) &= \frac{1}{2^n} \sum_{i_1=1}^2 \cdots \sum_{i_n=1}^2 \tilde{R}(t_1 + (-1)^{i_1} (t_1 - \tau_1), \dots, t_n + (-1)^{i_n} (t_n - \tau_n)) \prod_{k=1}^n \frac{t_k - (-1)^{i_k} (t_k - \tau_k)}{t_k} \\ & \quad 0 \leq \tau_k \leq t_k, \quad k = 1, \dots, n \end{aligned} \tag{34}$$

For the sake of simplicity, $R_d(\boldsymbol{\tau})$ is first considered in 1D cases (i.e. $n = 1$) such that

$$R_d(\tau) = \frac{1}{2} \left(\tilde{R}(\tau) \frac{2t - \tau}{t} + \tilde{R}(2t - \tau) \frac{\tau}{t} \right), \quad 0 \leq \tau \leq t \tag{35}$$

As $R(\tau) \equiv R(-\tau) \Rightarrow \tilde{R}(\tau) \equiv R(\tau)$, we have

$$R_d(\tau) - R(\tau) = \frac{\tau}{2t} (R(2t - \tau) - R(\tau)), \quad 0 \leq \tau \leq t \tag{36}$$

Further noting that $R(\tau)$ in practice is monotone decreasing from the origin, the relation

$$\begin{aligned} R_d(\tau) - R(\tau) &= 0, \quad \tau = 0, t \\ R_d(\tau) - R(\tau) &\approx 0, \quad 0 < \tau < t \end{aligned} \tag{37}$$

holds when t is sufficiently large. Hence, for $\tau \in [-t, t]$, $H_d(x, \omega)$ provides a good estimate of $H(x, \omega)$ in the sense of the first two statistical moments.

For higher-dimensional cases, it can be proven using a similar procedure that, for $\tau \in \mathbf{T}^n$, $H_d(\mathbf{x}, \omega)$ provides a good estimate of $H(\mathbf{x}, \omega)$ as long as \mathbf{T}^n is sufficiently large and $H(\mathbf{x}, \omega)$ is isotropic or orthotropic. The isotropic/orthotropic requirement of $H(\mathbf{x}, \omega)$ is because, although $R(\tau) \equiv R(-\tau)$ holds for any real-valued 2D/3D stationary stochastic fields, $\tilde{R}(\tau) = R(\tau)$ holds only for isotropic or orthotropic 2D/3D stationary stochastic fields.

The advantage of the diagonal F–K–L approximation (32) is its inexpensive computational cost as no equation solving is involved. It should also be noted that (32) does not provide the K–L solution of $H(\mathbf{x}, \omega)$, $\mathbf{x} \in \mathbf{T}^n$. For large random media with small effective correlation length, the full F–K–L discretization scheme requires the solution of a large algebraic eigenvalue problem, which may be beyond the available computer storage (especially in 3D cases). For those ‘unsolvable’ situations, the diagonal F–K–L approximation scheme may provide an acceptable alternative.

4.2. Estimates of the eigenvalue decay

In an SFEM formulation, the size of the final algebraic equation system or the number of necessary parametric simulations is determined by the total number of random variables included in the mathematical model. Generally, the more the random variables in the model, the more the computing power required to solve the associated stochastic PDEs. Hence, when the K–L expansion is employed to discretize random material properties, it is desirable to have an approximate prediction on the eigenvalue decay, which in turn determines the total number of random variables included in the simulation system.

Let λ_i/λ_1 denote the eigenvalue decay rate. In the F–K–L discretization scheme, λ_i/λ_1 can be readily predicted by two different methods.

In the first method, λ_i/λ_1 is estimated by using the spectral density function $f(\mathbf{y})$. Specifically, through a procedure similar to the derivation of (14)–(16),

$$\frac{\lambda_i}{\lambda_1} \approx \frac{f\left(m_{i1}\frac{\pi}{t_1}, \dots, m_{in}\frac{\pi}{t_n}\right)}{f(\mathbf{0})}, \quad i \geq 1 \quad (38)$$

From the above predication, it is clear that the larger the random medium domain \mathbf{T}^n , the slower the decay of eigenvalues, and *vice versa*. In addition, according to Equation (8) and the Heisenberg inequality [25], a smaller effective correlation length normally corresponds to a wider spectral density function $f(\mathbf{y})$, and therefore resulting in slower eigenvalue decay, and *vice versa*.

In the second prediction method, according to property (31), λ_i/λ_1 can be estimated using the diagonal entries of \mathbf{G} . Specifically, according to (20)–(23),

$$\frac{\lambda_i}{\lambda_1} \approx \frac{\int_0^{2t_1} \dots \int_0^{2t_n} \tilde{R}(\tau) \left(\prod_{k=1}^n \left(2 - \frac{\tau_k}{t_k} \right) \cos \left(m_{ik} \frac{\pi}{t_k} \tau_k \right) \right) d\tau}{\int_0^{2t_1} \dots \int_0^{2t_n} \tilde{R}(\tau) \prod_{k=1}^n \left(2 - \frac{\tau_k}{t_k} \right) d\tau}, \quad i \geq 1 \quad (39)$$

In the above prediction, the eigenvalues are estimated by the Fourier coefficients of the axis-symmetric component of $\tilde{R}(\tau) \prod_{k=1}^n (2 - \tau_k/t_k)$. Hence, the eigenvalue decay rate λ_i/λ_1 is approximately the decay rate of some Fourier coefficients.

Let $c_j(g)$, $j = 0, \pm 1, \pm 2, \dots$ be the Fourier coefficients of a function $g(x)$ defined in an interval. It is well known in the classic theory of Fourier series [29] that

- (1) If g has a finite total variation $V(g)$, then $|c_j(g)| \leq V(g)/|4j|$.
- (2) If the p th derivative of g is absolutely continuous, then $c_j(g) = o(1/|j|^{p+1})$ as $j \rightarrow \pm\infty$.

Consequently, in 1D cases, λ_i/λ_1 is at least proportional to $1/i$ (for sufficiently large i) as long as the corresponding condition of the bounded variation is satisfied; moreover, the smoother the covariance function, the faster the eigenvalues decay. The generalization of these conclusions to higher-dimensional cases with separable $\tilde{R}(\boldsymbol{\tau})$ is immediate. For general higher-dimensional cases, although the analysis on Fourier coefficients is not straightforward, it can be expected that essentially similar estimates hold for λ_i/λ_1 .

4.3. Comparison with the Galerkin format using Fourier basis

The conventional K–L expansion of random material properties [12–18] is usually obtained by using the standard Galerkin FEM, in which the function basis is served by piecewise polynomials and, as indicated in Equation (4), the resulting algebraic system is a generalized eigenvalue problem. Recently, Li *et al.* [20] simply replaced piecewise polynomials with Fourier series in the Galerkin format and obtained a so-called Fourier representation for random material properties. Due to the orthogonality of Fourier series, the final algebraic system in [20] becomes a standard eigenvalue problem, which is formally the same as Equation (24). However, the Galerkin format using Fourier basis [20] did not yet resolve the computational problems highlighted in Section 1.2 and, specifically, compared with the F–K–L discretization scheme, it has the following weaknesses:

- Construction of the covariance matrix arising in [20] requires directly computing a number of integrations of multidimensional oscillatory functions, and as the matrix dimension grows the associated computational cost increases significantly, in particular in 2D and 3D problems.
- As the length of the Fourier series is determined by trial and error in [20], the approximation error of the random material properties discretized cannot be explicitly controlled in accordance with the given accuracy.
- In the Galerkin format using Fourier basis, there is no easy way to predict the decay speed of K–L eigenvalues. Hence, the total number of random variables required by the associated representation scheme of random material properties remains unknown until the final solutions of all K–L eigenpairs are obtained.

The above disadvantages are due to the fact that the spectral representation theory [5–8], which plays an important role in this paper, has not been taken into consideration in the Galerkin format using the Fourier basis [20].

5. NUMERICAL EXAMPLES

In this section, the overall performance of the F–K–L discretization scheme is first examined through two examples, and then an underground tunnel application is presented to demonstrate its use in SFEM analysis.

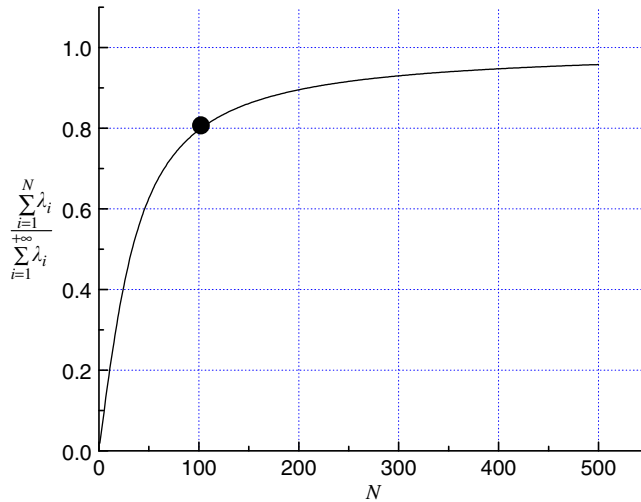


Figure 2. Asymptotic property of eigenvalues (Case I).

In this paper, the effective correlation length of a stationary stochastic field $H(\mathbf{x}, \omega)$, $\mathbf{x} \subset D$ with covariance function $R(\mathbf{x}_1 - \mathbf{x}_2)$ is defined as the minimum value τ_c such that $R(\mathbf{x}_1 - \mathbf{x}_2) \leq R(\mathbf{0})/100$ holds for all points $\mathbf{x}_1, \mathbf{x}_2 \in D$ satisfying $\|\mathbf{x}_1 - \mathbf{x}_2\|_2 > \tau_c$. Furthermore, without loss of generality, it is assumed that $H_0(\mathbf{x}) = H_0 = 0$ in the first two examples.

5.1. Example 1: stationary random material properties in 1D problems

Two stationary stochastic fields that are widely used in the description of random material properties are considered:

- *Case I:* $H_{1D}^1(x, \omega)$, $x \in [-t, t]$ with covariance function $e^{-|x|/a_1}$, $a_1 > 0$.
- *Case II:* $H_{1D}^2(x, \omega)$, $x \in [-t, t]$ with covariance function e^{-x^2/a_2} , $a_2 > 0$.

5.1.1. *Case I.* Although $H_{1D}^1(x, \omega)$ has been widely used in the SFEM literature (e.g. [3, 4, 6, 7, 12, 13, 15, 17, 18]), the authors do not advocate its use in describing the material properties of random media because it is non-differentiable almost everywhere [22, 23]. The *sole* objective of choosing $H_{1D}^1(x, \omega)$ is to investigate the accuracy of the proposed F–K–L discretization scheme.

Assuming $t = 65$ and $a_1 = 1.25$, the effective correlation length of $H_{1D}^1(x, \omega)$ is 5.75. The K–L expansion of $H_{1D}^1(x, \omega)$ is, obtained using the exact solution (see e.g. [11, 13]), the FEM (see e.g. [13, 18]) and the proposed F–K–L discretization scheme. Figure 2 plots $\sum_{i=1}^N \lambda_i / \sum_{i=1}^{+\infty} \lambda_i$ against N , in which $\sum_{i=1}^{+\infty} \lambda_i = 130$ and λ_i are calculated from the exact solution. It is observed that the K–L expansion requires the first $N = 100$ eigenpairs to approximate 80% of the total variance of $H_{1D}^1(x, \omega)$, i.e. $\sum_{i=1}^N \lambda_i / \sum_{i=1}^{+\infty} \lambda_i = 0.8$.

Indeed, the number of terms contained in a reasonable K–L expansion of a random material property encountered in practice can easily reach a few hundred, even in 1D problems. This is because the ratio of the random medium size to the effective correlation length can be even larger

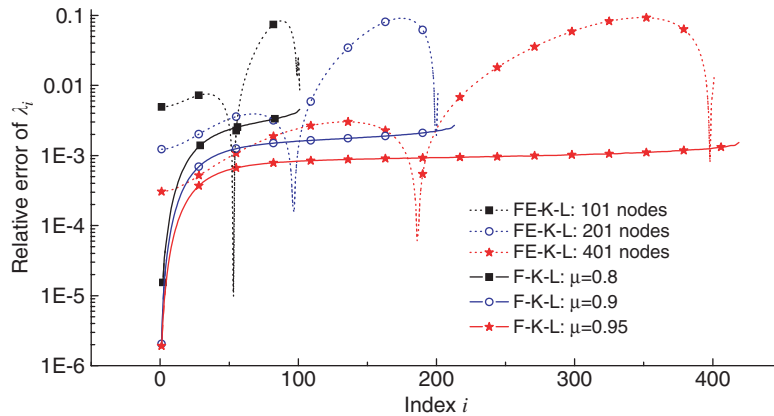


Figure 3. Relative errors of eigenvalues (Case I).

than that in this simple example. Hence, in order to achieve a reasonable K–L expansion of the stochastic field concerned, it is important to accurately obtain all the required eigenvalues and eigenfunctions rather than only the first few eigenpairs.

The relative errors of K–L eigenvalues are compared in Figure 3, in which the curves labelled F–K–L are obtained with the F–K–L discretization scheme and the curves labelled FE–K–L are obtained with the FEM. It is observed that the eigenvalue accuracy of the F–K–L discretization scheme is much higher than that of the FE-mesh-based K–L expansion. Specifically, in the F–K–L scheme, the approximation error is explicitly controlled by μ and all eigenvalues are obtained with good accuracy; however, in the FE–K–L scheme, only half of the eigenvalues are obtained with reasonable accuracy.

Figure 4 compares some eigenfunctions of $H_{1D}^1(x, \omega)$ and, as expected, the F–K–L scheme shows a significant advantage over the FE–K–L solution. Although the accuracy of the FE-mesh-based K–L solution can be improved by employing more elements, the FE–K–L solution in general provides relatively poor results for higher-order eigenfunctions. In the F–K–L solution with $\mu = 0.8$, the dimensionality of the covariance matrix \mathbf{G} is only 100; however, for the eigenfunctions shown in Figure 4, there is no visible difference between the associated F–K–L solution and the exact solution up to the 80th eigenfunction.

5.1.2. Case II. The aim of this particular example is to investigate the influences of the random medium size and the effective correlation length on the F–K–L discretization scheme. Letting $a_2 = 2$, the effective correlation length of $H_{1D}^2(x, \omega)$ is 3.0. Consider $H_{1D}^2(x, \omega)$ defined in $[-1.5r, 1.5r]$, where $r \in \{5, 10, 15, 20\}$ denotes the ratio of the interval size to the effective correlation length.

The K–L expansion of $H_{1D}^2(x, \omega)$ is obtained with the F–K–L discretization scheme, with $\mu = 0.95$. The covariance-matrix property (31) is verified in Figure 5, where the matrix elements are linearly mapped into pixels whose colours represent the values of the corresponding entries. It is observed that inequality (31) holds well in various cases with different ratios r .

Figure 6 plots the eigenvalue decay rate λ_i/λ_1 , in which scatters $\blacksquare \square \blacktriangle \triangle$ are directly calculated from the eigenvalues, and the solid and dashed curves are predicted using, respectively, (38)

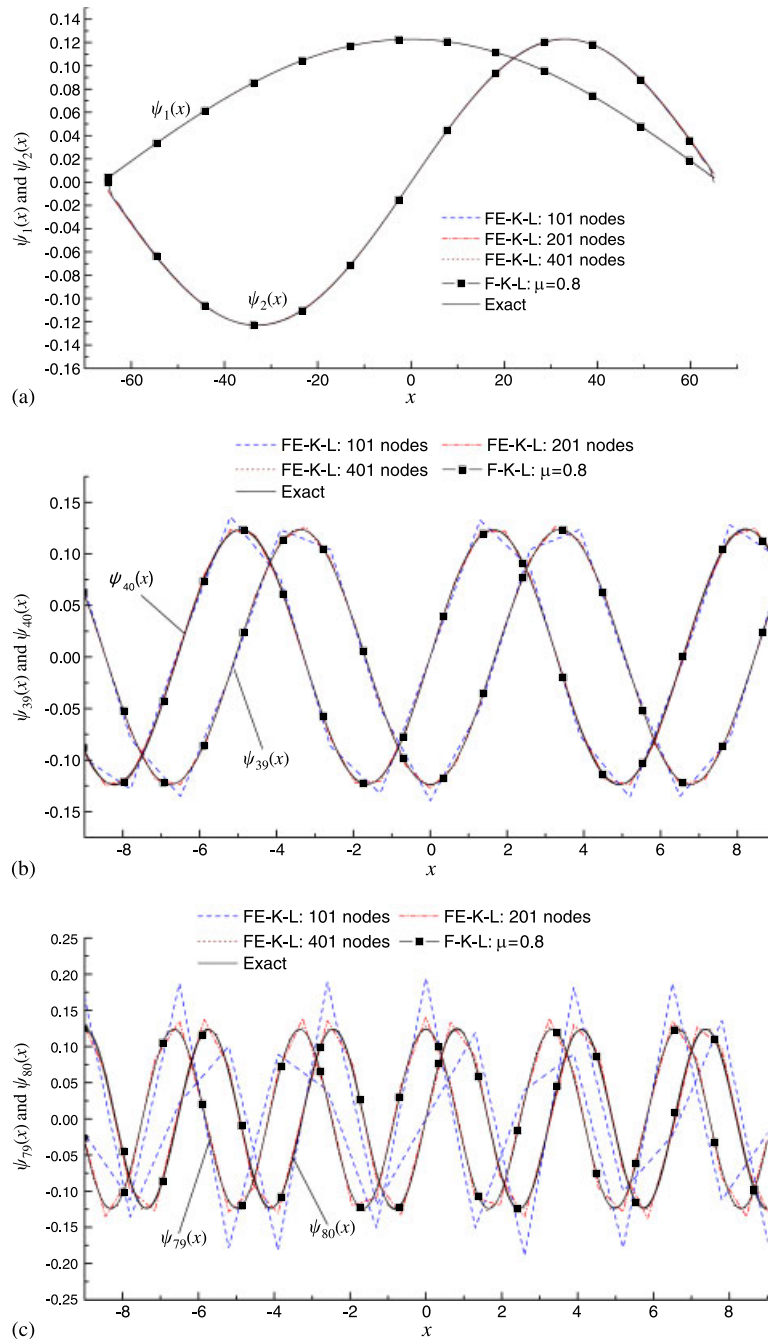


Figure 4. Comparison of eigenfunctions (Case I).

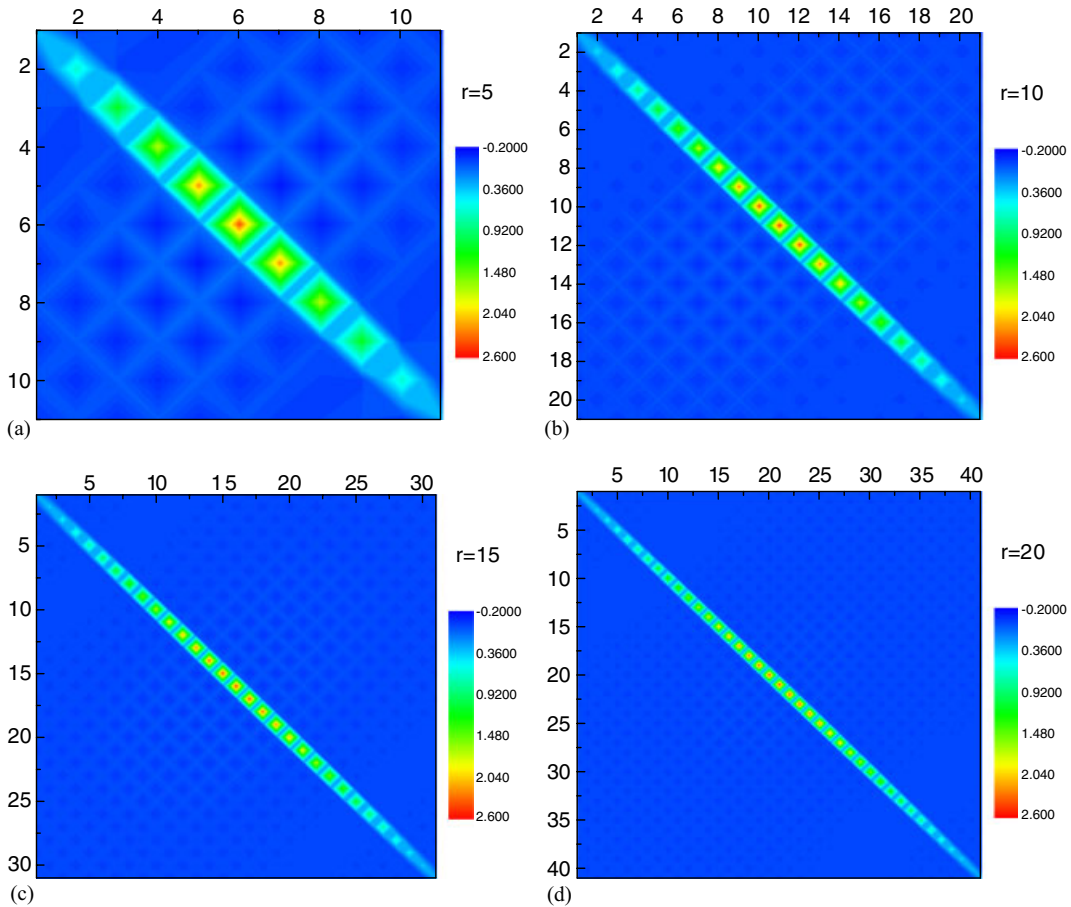


Figure 5. The covariance matrix \mathbf{G} (Case II).

and (39). As expected, the larger the ratio r , the slower the decay of eigenvalues. Both the spectral density function prediction and the diagonal entry prediction provide good estimates of the eigenvalue decay rate.

To examine the diagonal F-K-L approximations of $H_{1D}^2(x, \omega)$, Figure 7 compares their covariance functions with the exact covariance function $e^{-\tau^2/2}$, and achieves reasonable agreements in $\tau \in [-1.5r, 1.5r]$.

5.2. Example 2: stationary random material properties in 2D problems

This example considers the random material property described by a general stationary stochastic field $H_{2D}(\mathbf{x}, \omega)$, $\mathbf{x} \in [-15, 15] \times [-15, 15]$ with an inseparable covariance function $e^{-(\tau_1^2/3 + \tau_2^2/4)^{2/3}}$. The effective correlation length of $H_{2D}(\mathbf{x}, \omega)$, is 6.3.

As no exact K-L solution is available for $H_{2D}(\mathbf{x}, \omega)$, only the F-K-L discretization is constructed for this general stationary stochastic field. By setting $\mu = 0.95$ in the F-K-L discretization scheme

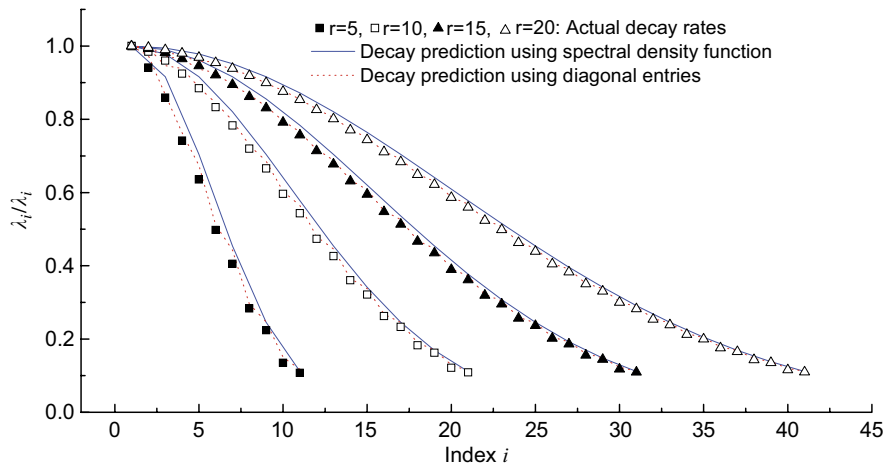


Figure 6. Eigenvalue decay rates (Case II).

are around 2800 K–L eigenpairs obtained for $H_{2D}(\mathbf{x}, \omega)$. In a PC system with an Intel Xeon 2.4 GHz processor and 1.0 GB DDR memory it takes 23.6 s to construct the block-diagonal covariance matrix \mathbf{G} , and with the standard MATLAB eigensolver it takes 216.2 s to solve for the entire algebraic eigenstructure of \mathbf{G} .

Figures 8 and 9 plot, respectively, the eigenvalues and eigenfunctions, and Figure 10 shows a particular realization of $H_{2D}(\mathbf{x}, \omega)$, which is generated from the obtained F–K–L discretization with $\mu^* = 0.8$.

5.3. Example 3: an underground tunnel application

An underground rock tunnel is investigated using a simple plain-strain model. The geometrical configuration and boundary conditions are shown in Figure 11, and the Young's modulus is described by a stationary stochastic field with a mean value $H_0 = 3.0 \times 10^{10}$ Pa and a covariance function $R(\tau) = 3.8025 \times 10^{20} e^{-[(x_2-x_1)^2+(y_2-y_1)^2]}/2.0^2 \text{ Pa}^2$.

First, by using the F–K–L discretization scheme, the random Young's modulus is expressed in the form of Equation (29). Then, following a standard FEM procedure, a stochastic linear system

$$(\xi_1(\omega)\mathbf{K}_1 + \xi_2(\omega)\mathbf{K}_2 + \cdots + \xi_{N^*}(\omega)\mathbf{K}_{N^*})\mathbf{u}(\omega) = \mathbf{P} \quad (40)$$

is constructed, in which $\xi_i(\omega)$ are the random variables in the F–K–L discretization of Young's modulus, \mathbf{K}_i the corresponding deterministic stiffness matrices, \mathbf{P} the deterministic nodal-load vector and $\mathbf{u}(\omega)$ the unknown random nodal-displacement vector.

The solution $\mathbf{u}(\omega)$ is explicitly obtained after simultaneously diagonalizing all matrices \mathbf{K}_i in the stochastic linear system. The details of this novel joint-diagonalization solution strategy have been reported previously [19].

Corresponding to one particular variation in the random Young's modulus, principal stress distributions of the stochastic plain-strain model are plotted in Figure 12. It is observed that, besides the influence from the deterministic geometrical configurations and external loads, which is represented by the symmetric stress concentration around the tunnel, the stress distributions are

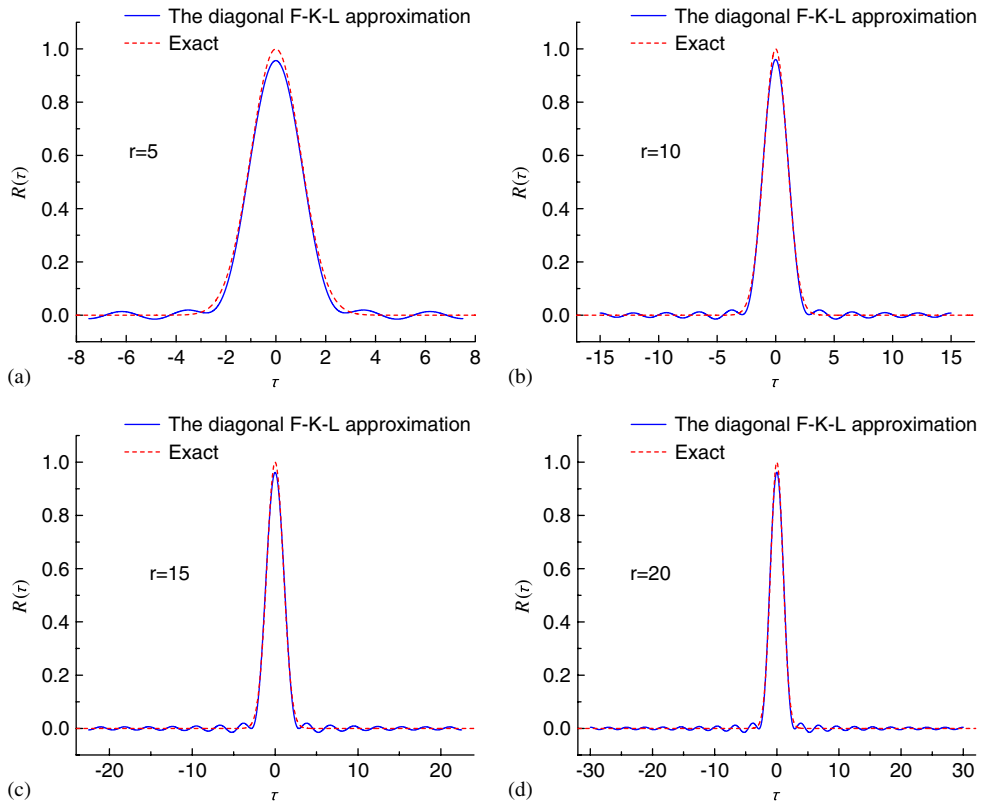


Figure 7. Accuracy of the diagonal F-K-L approximation scheme (Case II).

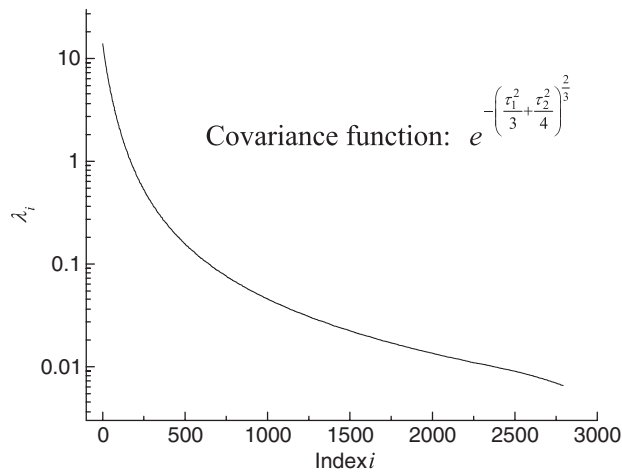


Figure 8. The eigenvalues of $H_{2D}(\mathbf{x}, \omega)$.

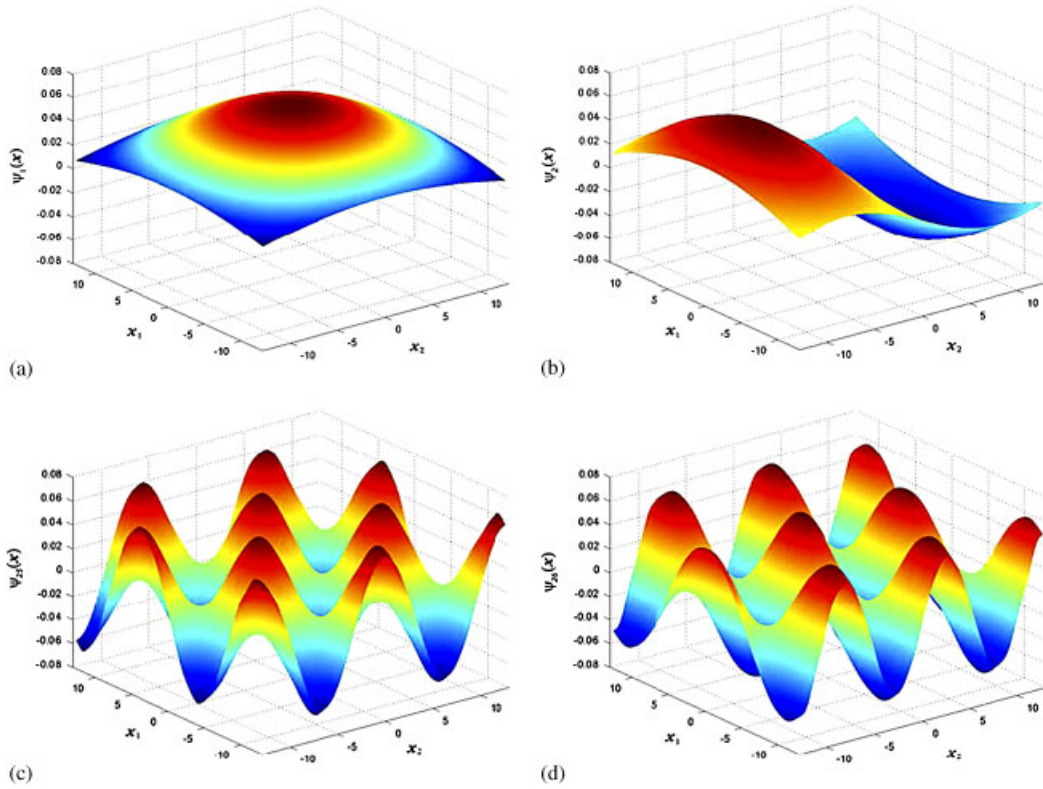


Figure 9. The eigenfunctions of $H_{2D}(x, \omega)$.

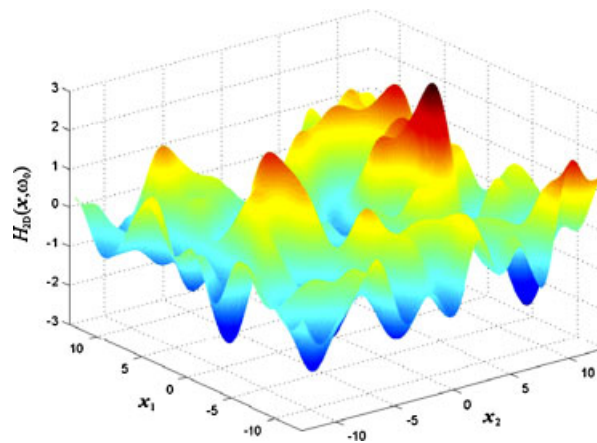


Figure 10. A particular realization of $H_{2D}(x, \omega)$.

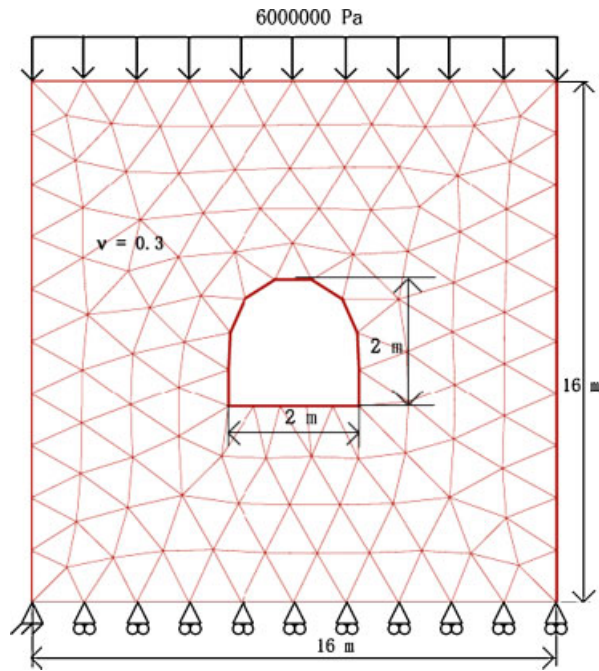


Figure 11. Illustration of Example 3.

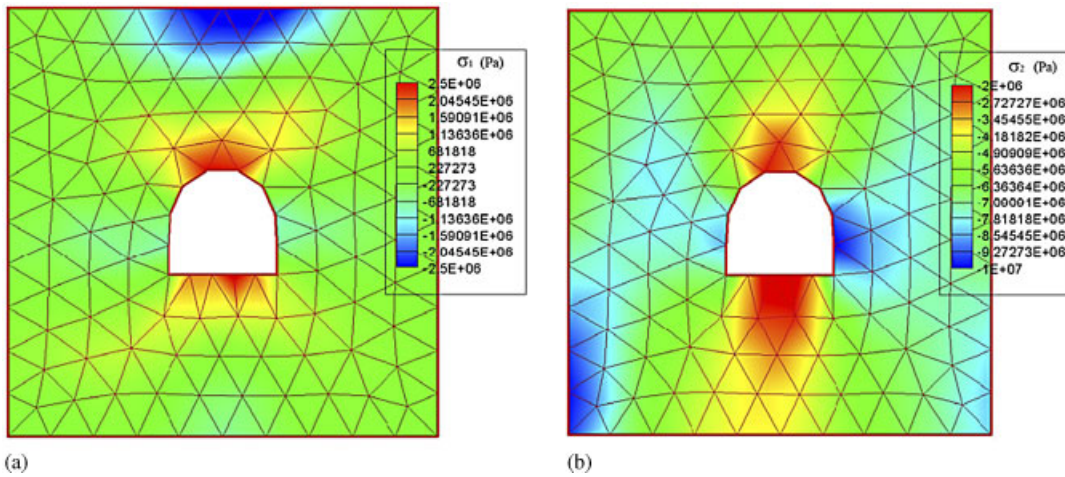


Figure 12. Principal stress distributions of a simplified tunnel model (one-sample path): (a) principal stress σ_1 and (b) principal stress σ_2 .

also strongly influenced of by the random distribution of Young's modulus, which is reflected by the irregular variation in principal stresses through the medium. To arrive at a rational analysis conclusion, the stress distributions should be summarized in a probability context to take into consideration all possible pathwise solutions.

6. CONCLUSIONS

Utilizing the connection between the K–L expansion theorem and the spectral representation theory, an F–K–L discretization scheme for stationary random material properties is developed to overcome the computational difficulties arising from the application of K–L expansions in the SFEM analysis, and a number of technical challenges encountered in the development are solved.

Compared with the FE-mesh-based K–L expansion scheme that has, to a large extent, become the standard method for the discretization of random material properties in SFEM simulations, the proposed discretization scheme possesses the following advantages:

- The computational cost is very competitive, in that its underlying algebraic system is a standard eigenvalue problem with respect to a block-diagonal real symmetric matrix that can be readily formed by using the standard FFT. Also, in cases where the matrix involved exceeds the computer storage, an alternative diagonal F–K–L approximation scheme can be explicitly constructed without solving any equation.
- A priori error-control mechanism is provided. Specifically, the approximation error of random material properties is explicitly controlled by two parameters, which control, respectively, the error of K–L eigenpairs and of the total variance.
- Due to the harmonic essence of stationary random material properties, the accuracy of the F–K–L discretization scheme is much better than that of the primitive K–L expansion scheme.
- Two accurate methods are equipped in the scheme to predict the associated eigenvalue-decay speed, which in turn makes it possible to estimate precisely the overall computational cost of an SFEM analysis before the simulation starts.
- It is completely meshfree and also independent of the detailed shape of the random structure.

It is worth mentioning that, for a stationary random material property $H(\mathbf{x}, \omega)$, $\mathbf{x} \in \mathbf{T}^n$, some eigenfunctions obtained by the F–K–L discretization scheme do not converge to the exact eigenfunctions near $\partial\mathbf{T}^n$, i.e. the boundary of \mathbf{T}^n . This is due to the Gibbs phenomenon [29], where some eigenfunctions of $H(\mathbf{x}, \omega)$ have discontinuities on $\partial\mathbf{T}^n$. This adverse phenomenon can be overcome by adjusting the Fourier summation with Lanczos' σ factor [30] or by slightly extending the computational domain of \mathbf{T}^n .

ACKNOWLEDGEMENT

This work is supported by the EPSRC of U.K. under grant nos GR/R87222 and GR/R92318. This support is gratefully acknowledged.

REFERENCES

1. Shinozuka M. Monte Carlo solution of structural dynamics. *Computers and Structures* 1972; **2**(5–6):855–874.
2. Yamazaki F, Shinozuka M, Dasgupta G. Neumann expansion for stochastic finite element analysis. *Journal of Engineering Mechanics* (ASCE) 1988; **114**(8):1335–1354.
3. Vanmarcke EH, Grigoriu M. Stochastic finite element analysis of simple beams. *Journal of Engineering Mechanics* (ASCE) 1983; **109**(5):1203–1214.
4. Liu WK, Belytschko T, Mani A. Random field finite-elements. *International Journal for Numerical Methods in Engineering* 1986; **23**(10):1831–1845.
5. Kamiński M, Kleiber M. Stochastic structural interface defects in fiber composites. *International Journal of Solids and Structures* 1996; **33**(20–22):3035–3056.

6. Hien TD, Kleiber M. Stochastic finite element modelling in linear transient heat transfer. *Computer Methods in Applied Mechanics and Engineering* 1997; **144**(1–2):111–124.
7. Li CC, Derkiureghian A. Optimal discretization of random fields. *Journal of Engineering Mechanics* (ASCE) 1993; **119**(6):1136–1154.
8. Shinozuka M, Deodatis G. Simulation of stochastic processes by spectral representation. *Applied Mechanics Reviews* (ASME) 1991; **44**(4):191–204.
9. Hurtado JE, Barbat AH. Monte Carlo techniques in computational stochastic mechanics. *Archives of Computational Methods in Engineering: State of the Art Reviews* 1998; **5**(1):3–30.
10. Grigoriu M. A spectral representation based model for Monte Carlo simulation. *Probabilistic Engineering Mechanics* 2000; **15**:365–370.
11. Grigoriu M. *Stochastic Calculus: Applications in Science and Engineering*. Birkhauser: Basel, 2002.
12. Spanos PD, Ghanem RG. Stochastic finite element expansion for random media. *Journal of Engineering Mechanics* (ASCE) 1989; **115**(5):1035–1053.
13. Ghanem RG, Spanos PD. *Stochastic Finite Elements: A Spectral Approach* (Revised edn). Dover: New York, 2003.
14. Ghanem RG. Ingredients for a general purpose stochastic finite elements implementation. *Computer Methods in Applied Mechanics and Engineering* 1999; **168**:19–34.
15. Matthies HG, Bucher C. Finite elements for stochastic media problems. *Computer Methods in Applied Mechanics and Engineering* 1999; **168**(1–4):3–17.
16. Matthies HG, Keese A. Galerkin methods for linear and nonlinear elliptic stochastic partial differential equations. *Computer Methods in Applied Mechanics and Engineering* 2005; **194**(12–16):1295–1331.
17. Babuška IM, Chatzipantelidis P. On solving elliptic stochastic partial differential equations. *Computer Methods in Applied Mechanics and Engineering* 2002; **191**(37–38):4093–4122.
18. Frauenfelder P, Schwab C, Todor RA. Finite elements for elliptic problems with stochastic coefficients. *Computer Methods in Applied Mechanics and Engineering* 2005; **194**(2–5):205–228.
19. Li CF, Feng YT, Owen DRJ. Explicit solution to the stochastic system of linear algebraic equations $(\alpha_1 \mathbf{A}_1 + \alpha_2 \mathbf{A}_2 + \dots + \alpha_m \mathbf{A}_m) \mathbf{x} = \mathbf{b}$. *Computer Methods in Applied Mechanics and Engineering* 2006; **195**:6560–6576.
20. Li CF, Feng YT, Owen DRJ *et al.* Fourier representation of random media fields in stochastic finite element modelling. *Engineering Computations* 2006; **23**(7):794–817.
21. Loève M. *Probability Theory* (4th edn), vol. 2. Springer: Berlin, 1977.
22. Yaglom AM. *An Introduction to the Theory of Stationary Random Functions*. Prentice-Hall: Englewood Cliffs, NJ, 1962.
23. Adler RJ. *The Geometry of Random Fields*. Wiley: New York, 1981.
24. Van Trees HL. *Detection, Estimation, and Modulation Theory, Part I* (Paperback edn). Wiley: New York, 2001.
25. Dym H, McKean HP. *Fourier Series and Integrals*. Academic Press: New York, 1972.
26. Jolliffe IT. *Principal Component Analysis* (2nd edn). Springer: New York, 2002.
27. Davis PJ, Rabinowitz P. *Methods of Numerical Integration*. Academic Press: New York, 1984.
28. Press WH, Teukolsky SA, Vetterling WT *et al.* *Numerical Recipes in C: The Art of Scientific Computing* (2nd edn). Cambridge University Press: Cambridge, 1995.
29. Edwards RE. *Fourier Series: A Modern Introduction*, vol. 1 (2nd edn). Springer: New York, 1979.
30. Hamming RW. *Numerical Methods for Scientists and Engineers* (2nd edn). Dover: New York, 1987.